Available online at www.sciencedirect.com
SCIENCE DIRECT
Journal of Catalysis 242 (2006) 103–109
JOURNAL OF CATALYSIS
www.elsevier.com/locate/jcat

Sintering inhibition mechanism of platinum supported on ceria-based oxide and Pt-oxide–support interaction

Yasutaka Nagai [a,*], Takeshi Hirabayashi [b], Kazuhiko Dohmae [a], Nobuyuki Takagi [b], Takashi Minami [c], Hirofumi Shinjoh [a], Shin'ichi Matsumoto [c]

[a] *TOYOTA Central R&D Labs., Inc., Nagakute, Aichi, 480-1192 Japan*
[b] *TOYOTA Motor Corporation Higashi-Fuji Technical Center, Shizuoka, 410-1193 Japan*
[c] *TOYOTA Motor Corporation, Toyota, Aichi, 471-8572 Japan*

Received 31 March 2006; revised 24 May 2006; accepted 2 June 2006

Available online 3 July 2006

Abstract

Sintering inhibition mechanism of Pt in Pt/ceria-based oxide catalyst under oxidizing condition at high temperature was studied by several analysis techniques. Pt in a Pt/ceria-based oxide catalyst did not sinter after aging treatment at 800 °C in air, but did sinter in a Pt/Al_2O_3 catalyst. Using X-ray absorption analysis, we found that the Pt–O–Ce bond (i.e., the Pt-oxide–support interaction) acted as an anchor and inhibited the sintering of Pt particles on ceria-based oxide. As a result of further systematic investigation on various Pt catalysts, clearly there was an excellent correlation between the strength of the Pt-oxide–support interaction and the electron density of oxygen in the support oxide. The sintering inhibition effect on Pt can be controlled by the electron density of oxygen in the support through the Pt-oxide–support interaction.

Keywords: Platinum; Sintering; Pt-oxide–support interaction; XAFS; Automotive catalyst

1. Introduction

Three-way catalysts (TWCs) can efficiently purify harmful automobile emissions. Ever since TWCs were commercialized in the U.S. and Japan in 1977 [1], they have played an important role in environmental protection. Recently, in concert with growing demands for global environmental protection, more stringent regulations have been imposed on automobile industries. Therefore, automobile companies are making strong efforts to clean up automobile exhaust, and technical innovation for more advanced TWCs needs to be encouraged.

Basically, a TWC consists of precious metals such as Pt and Rh, supports such as Al_2O_3, and ceria-based oxide as an oxygen storage component [2–4]. The precious metal particles are a few nanometers in diameter and are dispersed on a support oxide. These precious metals act as the active site to simultaneously purify harmful automotive exhaust, such as nitrogen oxides (NO_x), carbon monoxide (CO), and unburned hydrocarbons (HC). When the TWC is exposed to high temperatures (∼800 °C and above), the precious metal agglomerates and sinters, decreasing the active surface area [5–8]. Generally, the sintering of the precious metal particles during operation causes a decrease in catalytic activity (i.e., degradation). Moreover, exhaust conditions from an automotive gasoline engine fluctuate between oxidative and reductive atmospheres during vehicle operation. Specifically, the activity of Pt-supported catalysts decreases significantly after high-temperature aging in an oxidative atmosphere due to the sintering of Pt particles compared with that in a reductive atmosphere [5,6]. Therefore, the development of highly durable catalysts without Pt sintering in an oxidative atmosphere is highly desirable in automotive industrial research.

Ceria-based oxide is widely used for automotive catalysts because of its performance not only in storing/releasing oxygen, but also in stabilizing precious metal dispersion [2,9]. Several studies have been conducted on the Pt sintering and Pt–support interaction in Pt/ceria catalysts, and significant progress

* Corresponding author. Fax: +81 561 63 6150.
E-mail address: e1062@mosk.tytlabs.co.jp (Y. Nagai).

0021-9517/$ – see front matter
doi:10.1016/j.jcat.2006.06.002

in knowledge has been made. Diwell et al. [10] reported that formation of a Pt–ceria complex under oxidizing conditions could maintain Pt stability against sintering. In addition, using a laser Raman technique, Murrell et al. [11] showed that the precious metal oxide structure interacts strongly with the ceria surface. However, the nature of the Pt–ceria interaction remains very complicated, and there is room for further investigation.

In this paper we explore the sintering inhibition mechanism of Pt particles on ceria-based oxide at the atomic level using X-ray absorption analysis. Then we conduct further systematic investigation on various Pt catalysts and clarify the essence of the Pt-oxide–support interaction and its relationship to Pt sintering in an oxidizing atmosphere.

2. Experimental

2.1. Catalyst preparation and aging treatment

Pt/Al_2O_3 and Pt/ceria-based mixed oxide (Ce–Zr–Y mixed oxide, referred to as CZY) catalysts were prepared by the following methods. Al_2O_3 as a support oxide was supplied by Nikki Universal; its crystal structure was γ-type. CZY powder as a support oxide was prepared using a coprecipitation process with aqueous NH_3 using $Ce(NO_3)_3$, $ZrO(NO_3)_2$, and $Y(NO_3)_3$ in aqueous solutions. The precipitate was dried at 110 °C and calcined in air at 700 °C for 3 h. CZY contains 50 wt% CeO_2, 46 wt% ZrO_2, and 4 wt% Y_2O_3, and its crystal structure is cubic. Preparation of 2 wt% Pt/Al_2O_3 and 2 wt% Pt/CZY catalysts was done by the conventional wet impregnation of Al_2O_3 and CZY powders with $Pt(NH_3)_2(NO_2)_2$ aqueous solution. The impregnated powders were dried overnight at 110 °C and calcined at 500 °C for 3 h in air. These samples are referred to as "fresh catalyst." Portions of the fresh sample were aged in air for 5 h at 800 °C. This aging treatment corresponds to an accelerated test for durability in an oxidative atmosphere. These samples are referred to as "aged catalysts." Pt/SiO_2, Pt/ZrO_2, Pt/TiO_2, and Pt/CeO_2 for a systematic study were prepared by the aforementioned method, using commercial support oxides, and aged as just described.

The aged Pt/CZY was reduced by 5% H_2 (N_2 balance) at 400 °C for 30 min. The reduced sample was cooled to room temperature, then placed in a bag with an oxygen scavenger to avoid oxidation. Aged and fresh samples were placed into a bag without an oxygen scavenger. The samples in the bag were used for the XAFS experiments.

2.2. Characterization

2.2.1. Adsorption methods

The specific surface areas of the samples were estimated using the N_2 adsorption isotherm at −196 °C by the one-point Brunauer–Emmett–Teller (BET) method using an automatic surface analyzer (Micro Sorp 4232II, Micro Data). The samples were pretreated in flowing N_2 at 200 °C for 20 min. The BET surface areas of the fresh and aged catalysts examined for this study, along with information on the support, are summarized in Table 1.

Table 1
The catalyst samples and BET surface area

Sample[a]	Pt loading (wt%)	Support	BET surface area (m^2/g)	
			Fresh catalyst	Aged catalyst[b]
Pt/Al_2O_3	2	γ-Al_2O_3	185	154
Pt/CZY	2	Ce–Zr–Y mixed oxide, cubic-type, 50 wt% CeO_2–46 wt% ZrO_2–4 wt% Y_2O_3	99	58
Pt/CeO_2	2	Cubic-type CeO_2	107	81
Pt/SiO_2	2	Amorphous SiO_2	51	47
Pt/ZrO_2	2	Tetragonal + monoclinic-type ZrO_2	87	30
Pt/TiO_2	2	Rutile-type TiO_2	67	34

[a] For sample description, see Section 2.
[b] Fresh samples were aged in air for 5 h at 800 °C.

The average particle size of Pt metal was determined using a CO pulse adsorption method [12]. The catalysts were pretreated in flowing pure oxygen, followed by pure hydrogen at 400 °C. With this reductive treatment of hydrogen, Pt was reduced to Pt metal. CO pulse adsorption was carried out in flowing He at −78 °C. At this temperature, CO uptake on ceria support was almost entirely suppressed, and CO was adsorbed to only the surface of Pt [13]. The average particle size was calculated from the CO uptake assuming that CO was adsorbed on the surface of spherical Pt particles at CO/(surface Pt atom) = 1/1 stoichiometry.

2.2.2. Structure analysis

Microstructure of the catalysts was investigated by transmission electron microscopy (TEM) using a JEOL JEM-2000EX. The powder XRD experiments were carried out in air at room temperature using a RINT2000 (Rigaku) diffractometer with Cu$K\alpha$ radiation (1.5406 Å). The catalyst samples were reduced by 5% H_2 (N_2 balance) at 400 °C for 30 min before the XRD measurements. The catalyst powder was pressed into wafers and affixed to standard-sized microscope slides. The average particle size of Pt was estimated from the Pt(111) line width using Scherrer's equation with the Gaussian line shape approximation.

The Pt L_3-edge (11.5 keV) X-ray absorption fine structure (XAFS) measurement was carried out at BL01B1 and BL16B2 of SPring-8 (Hyogo, Japan). The storage ring energy was operated at 8 GeV with a typical current of 100 mA. The XAFS spectra at Pt L_3-edge were measured using a Si(111) double-crystal monochromator in fluorescence mode at room temperature in air. Data reduction of the XAFS was carried out as described elsewhere [14]. The curve-fitting analysis of the EXAFS spectra was performed for the inverse Fourier transforms on the Pt–oxygen and Pt–cation (cation = Pt, Ce, and Zr) shells using theoretical parameters calculated by McKale et al. [15].

The X-ray photoelectron spectroscopy (XPS) measurements were carried out using a PHI model 5500MC with Mg$K\alpha$ X-rays. The catalyst sample was placed on a grid and pretreated under 0.5 atm O_2 pressure at 500 °C for 5 min. The pretreated

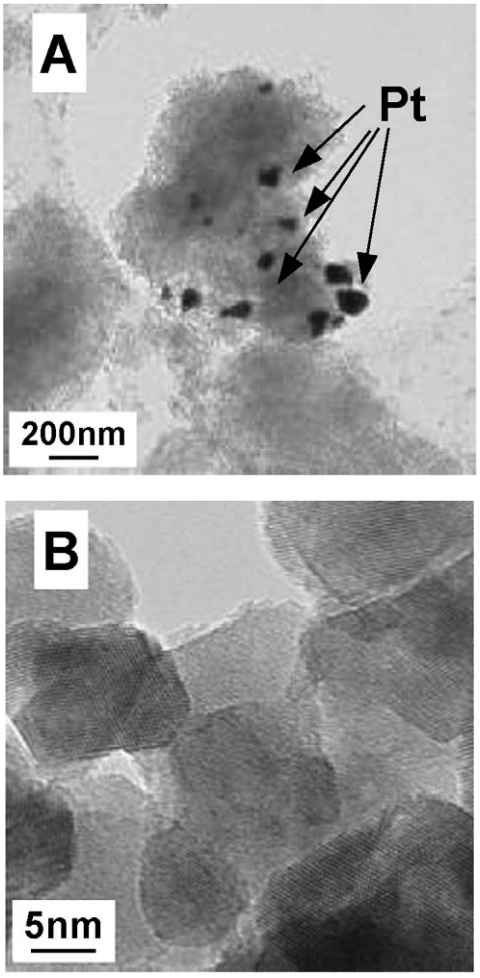

Fig. 1. TEM images of Pt supported catalysts after 800 °C aging in air for 5 h. (A) Pt/Al_2O_3 catalyst. (B) Pt/CZY (CZY denotes Ce–Zr–Y mixed oxide, see Section 2) catalyst.

sample was cooled to room temperature and then transferred to the XPS measurement stage without being exposed to air atmosphere. The oxygen 1s core electron levels in support oxides were recorded to evaluate the chemical property of the support. Binding energies were calibrated with respect to $Pt(4f_{7/2})$ at 71.4 eV.

3. Results and discussion

3.1. Sintering of Pt particles in Pt/Al_2O_3 and Pt/CZY catalysts

First, the Pt sintering behavior in Pt/Al_2O_3 and Pt/CZY catalysts was investigated. Fig. 1 shows the transmission electron microscopy (TEM) images of the Pt/Al_2O_3 and Pt/CZY catalysts after aging treatment at 800 °C in air for 5 h. In the aged Pt/Al_2O_3, large Pt particles ranging from 3 to 150 nm were observed. In contrast, no explicit Pt particles were observed on the aged Pt/CZY. In the aged Pt/CZY, Pt was detected by energy dispersive X-ray (EDX) analysis. This indicates that Pt particles are highly dispersed on the CZY support.

The average size of Pt metal particles for these catalysts was determined by XRD and the CO pulse method (Table 2). The

Table 2
Average platinum particle size of the catalysts estimated by XRD and CO pulse adsorption method

Sample		Average Pt particle size (nm)	
		XRD[a]	CO pulse
Pt/Al_2O_3	Fresh	ND[b]	1.0
	Aged	61	23.6
Pt/CZY	Fresh	ND[b]	1.1
	Aged	ND[b]	1.1

[a] Average particle size was estimated from Pt(111) line width.
[b] The diffraction peak from the Pt particles could not be detected.

diffraction peaks from the Pt particles in both fresh Pt/Al_2O_3 and Pt/CZY could not be detected by XRD because of their small particle size. Pt particle size on the Al_2O_3 support before the aging treatment, as estimated by the CO pulse method, was almost the same as that on CZY (about 1 nm diameter). This situation changed significantly after the aging. Pt particle size increased significantly in Pt/Al_2O_3 during the aging treatment; particle sizes in the aged Pt/Al_2O_3 determined by XRD and CO pulse methods were 61 and 23.6 nm, respectively. On the other hand, Pt particles in the Pt/CZY could not be observed by XRD even after aging, suggesting that the Pt particles on CZY support remained highly dispersed. The Pt particle size of 1.1 nm in the aged Pt/CZY estimated by CO pulse was the same as that in the fresh catalyst. This indicates that Pt in the Pt/CZY catalyst did not sinter at all after the aging treatment.

3.2. XAFS analysis of Pt/Al_2O_3 and Pt/CZY catalysts after aging

To clarify the cause of the inhibited sintering of Pt in Pt/CZY, the state of Pt atoms supported on Al_2O_3 or CZY was investigated by XAFS. Generally, the XAFS spectra can be divided into two spectral regions: the X-ray absorption near-edge structure (XANES) and extended X-ray absorption fine-structure (EXAFS) regions. We can get information on the electronic state from XANES analysis [16] and on the local structure around a target element from EXAFS analysis [17].

3.2.1. Pt L_3-edge XANES spectra

Fig. 2 shows the XANES spectra at Pt L_3-edge for the aged catalysts and reference samples. The steeply rising absorption edge is referred to as the "white line." In the case of the Pt L-edge XANES, the absorption intensity of the white line reflects the vacancy in the 5d orbital of Pt atoms [16]. A large white line was observed on oxidized Pt, whereas a small white line was observed on reduced Pt. Therefore, it is possible to estimate the average oxidation state of the Pt atoms in each sample. The white line intensity of Pt/Al_2O_3 was the same as that of Pt foil, suggesting that Pt on Al_2O_3 was in the Pt^0 (metal) state after aging. In contrast, the white line intensity of Pt/CZY was similar to that of PtO_2, suggesting that the Pt^{2+} and Pt^{4+} species with a high oxidation state were present mainly in the aged Pt/CZY. The average oxidation state of Pt can be quantitatively evaluated from the white line intensity [18]. A linear relationship exists between the white line intensity and the oxi-

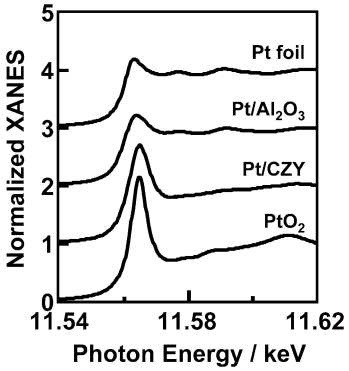

Fig. 2. Pt L_3-edge XANES spectra for supported Pt catalysts after 800 °C aging in air, together with standard samples of Pt foil and PtO_2 powder.

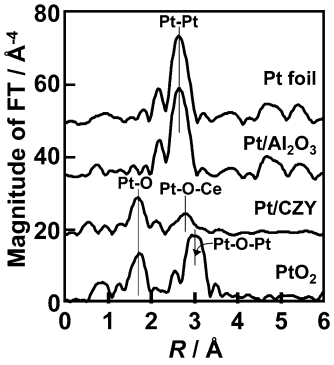

Fig. 3. Fourier-transformed k^3x data of Pt L_3-edge EXAFS for supported Pt catalysts after 800 °C aging in air and the standard samples of Pt foil and PtO_2 powder.

dation state of PtO_x on some metal oxide supports. On the basis of this linear relationship, the estimated oxidation state of Pt was 0 in the aged Pt/Al_2O_3 and 3.53 in the aged Pt/CZY.

Generally, it is well known that PtO_2 decomposes to Pt metal under oxidizing conditions at around 600 °C and above according to the thermodynamic phase diagram [19]. The finding that Pt on Al_2O_3 was in the Pt^0 state after aging at 800 °C in the oxidizing atmosphere was consistent with the thermodynamics. On the other hand, the CZY support could stabilize a high-oxidation state of Pt even after aging. Thus, it is suggested that the strong Pt–support interaction in the Pt/CZY under the oxidizing condition causes stabilization of the high-oxidation state of Pt.

3.2.2. *Fourier transforms of Pt L_3-edge EXAFS spectra*

Fourier transforms (FTs) of the aged catalysts and reference samples are presented in Fig. 3. The FTs were performed on the Pt L_3-edge EXAFS spectra in the ca. 3.0–16 $Å^{-1}$ region. The quantitative curve-fitting analysis of the EXAFS spectra was performed for the inverse FTs on the Pt–oxygen and Pt–cation (cation = Pt, Ce and Zr) shells, respectively. The results of curve-fitting analysis are summarized in Table 3. The FTs are not corrected for phase shift; therefore, the peaks in the FTs are shifted to lower R values. The values of bond length in the text and table are corrected for phase shift. In the FT spectrum of Pt foil, the peak at 2.76 Å is assigned to the Pt–Pt bond. In the

Table 3
Results of curve-fitting analysis for the aged catalysts and standard samples

Sample	Shell	CN	R (Å)	σ^2 ($Å^2$)
Pt foil[a]	Pt–Pt	12.0	2.76	0.0045
Pt/Al_2O_3	Pt–Pt	11.5	2.76	0.0046
Pt/CZY	Pt–O	4.1	2.02	0.0007
	Pt–Ce	3.5	3.01	0.0037
PtO_2[a]	Pt–O	5.7	2.04	0.0026
	Pt–Pt	5.3	3.10	0.0019

[a] The curve-fitting analysis for the standard samples were performed by reference to [23,24].

FT spectrum of PtO_2 powder, the peaks at 2.04 and 3.10 Å are assigned to the Pt–O and Pt–O–Pt bonds, respectively. The FT spectrum of Pt/Al_2O_3 after aging was obviously different from that of the Pt/CZY. As for the aged Pt/Al_2O_3, only the intense peak at 2.76 Å, which corresponds to the Pt–Pt bond, was observed. The FT spectrum of the Pt/Al_2O_3 coincided with that of Pt foil. The coordination number (CN) of the Pt–Pt shell in the aged Pt/Al_2O_3 was 11.5, indicating that the Pt metal particles on Al_2O_3 after aging were at least 20 nm in size [20]. The FT spectrum of Pt/CZY after aging differed from those of both Pt foil and PtO_2 powder. The position of the first peak at 2.02 Å in Pt/CZY was close to that of PtO_2, and this peak was fitted with the Pt–O bond. It should be noted that the second evident peak, which was absent in both Pt foil and PtO_2 powder, was found at 3.01 Å. A curve-fitting simulation of this second peak was carefully performed; Fig. 4 shows the results based on the supposition that the second neighboring atom was Ce or Pt. An excellent fitting result for the simulation of Ce was obtained. In contrast, an appropriate fit could not be obtained for Pt, because the EXAFS oscillation pattern of Pt was very different than that of the experimental data. It is clear that the second neighboring atom in the aged Pt/CZY is a Ce atom, not a Pt atom. Curve-fitting analysis for the simulation of other cations, such as Zr and Y, was also conducted to investigate the second neighboring atom in the aged Pt/CZY, but an appropriate fit for Ce compared with Zr(Y) could not be obtained. These results led to the conclusion that Pt atoms interact strongly with the CZY support during aging and form a Pt–O–Ce bond. The CN of the Pt–Ce shell in the aged Pt/CZY was 3.5. This CN of 3.5 is lower than the saturated CN of 12 in a cubic fluorite structure, indicating that Pt ions exist on the surface of the CZY support. In addition, intense Pt–Pt or Pt–O–Pt peaks could not be observed in the aged Pt/CZY, suggesting that there are no large Pt metal or oxide particles on the CZY. In other words, highly dispersed Pt oxides are present on the surface of the CZY support.

A similar Pt–O surface complex on CeO_2 has been reported by Murrell et al. [11], who stated that "using Laser Raman Spectroscopy, a strong Raman band at ca. 700 cm^{-1} was observed for Rh, Ir, Pd, and Pt dispersed on CeO_2. This Raman band was assigned to a surface oxide metal–O formed on the CeO_2 surface. Metal oxides on CeO_2 exhibit a Strong Oxide–Support Interaction (SOSI)." Our XAFS results could give direct evidence for the formation of a Pt–O–Ce bond on the surface of ceria-based oxide support. Moreover, we showed that

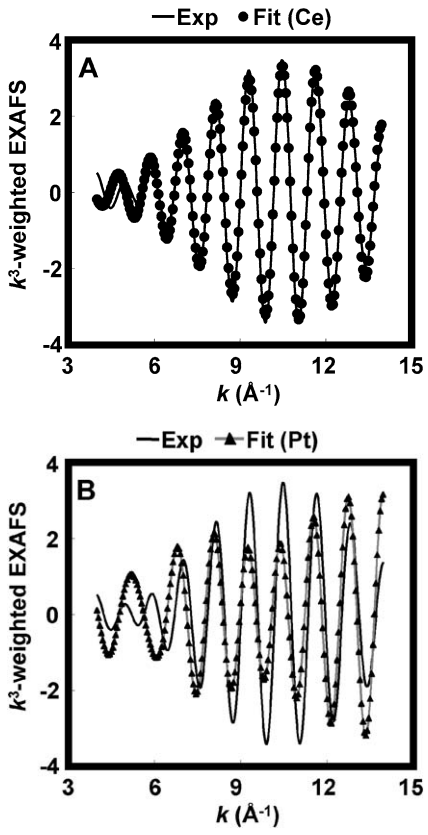

Fig. 4. The results of curve-fitting analysis on the inverse Fourier-transform of the second peak on the aged Pt/CZY catalyst in Fig. 3 and the corresponding curve-fit. (A) Experimental (—) and curve-fit on Ce atom (●). (B) Experimental (—) and curve-fit on Pt atom (–▲–).

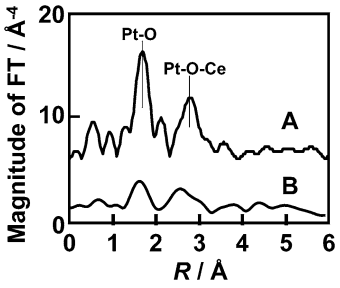

Fig. 5. Fourier-transformed k^3x data of Pt L_3-edge EXAFS for (A) Pt/CZY after 800 °C aging in air and (B) reduced Pt/CZY after aging.

this Pt-oxide–support interaction is stronger on the CZY surface than on the Al_2O_3 surface.

Generally, Pt^0 (metal) is considered to be the active site for the catalytic reaction in automotive exhaust conditions. The CZY support could stabilize a high-oxidation state of Pt after aging. Therefore, Pt on the CZY support must be reducible during the catalytic reaction. Fig. 5 shows the FTs of the aged Pt/CZY, which is the same spectrum mentioned in Fig. 3, and the reduced Pt/CZY after aging. The aged Pt/CZY was reduced by 5% H_2 at 400 °C. After the reductive treatment, the Pt–O peak in the aged Pt/CZY decreased significantly, and the Pt–O–Ce peak almost disappeared. In addition, intense Pt–Pt peak could not be observed in the reduced Pt/CZY. These results suggest that the Pt–O–Ce bond breaks by the reductive treatment and that Pt metal particles are highly dispersed on the CZY support. According to the results from the CO pulse method mentioned above, the estimated average size of Pt metal particles in the reduced Pt/CZY after the aging is ca. 1 nm.

3.3. Pt sintering inhibition mechanism

Based on our foregoing observations, we proposed the sintering inhibition mechanism of Pt supported on CZY shown in Fig. 6. In the case of Pt/Al_2O_3, because the interaction between Pt and Al_2O_3 is weak, Pt particles transport across the surface of the Al_2O_3 support and sinter during an aging treatment at 800 °C in an oxidizing atmosphere according to the molecular migration model [6,21,22]. In contrast, Pt supported on CZY has a strong interaction with the CZY support. Therefore, the CZY support stabilized a high-oxidation state of Pt, and then the formation of the rigid Pt–O–Ce bond acts as an anchor. Formation of the Pt–O–Ce bond on the CZY suppresses the sintering of Pt. The highly dispersed Pt oxide on the surface of CZY support under oxidizing conditions is considered to be more stable, because the Pt–O–Ce bond energies are greater than the Pt–Pt bond energies in large Pt crystallites. In contrast, during catalytic reactions under stoichiometric or reducing conditions, the Pt–O–Ce bond on the CZY breaks, and Pt metal particles are highly dispersed on the support.

It is well known that the sintering of supported metal not only occurs via the foregoing metal migration, but also decreases in the support surface area during aging [6,21,22]. The surface areas of the fresh and aged Pt/Al_2O_3 were 185 and 154 m^2/g, respectively (Table 1). In contrast, the surface area of Pt/CZY decreased from 99 to 58 m^2/g, as shown in Table 1. The aging treatment resulted in a 40% decrease in the surface area of Pt/CZY. Although the Al_2O_3 support has a high thermal stability compared with the CZY support, Pt particles on the Al_2O_3 support sintered significantly. Therefore, the Pt sintering was due mainly to Pt migration, not to the decreased surface area of the support. As for the sintering inhibition mechanism, the Pt–O–Ce bond (i.e., the Pt-oxide–support interaction) inhibits Pt migration, which is the main reason why Pt supported on CZY does not sinter during the high-temperature aging in oxidative atmosphere.

3.4. Inhibition effect of Pt sintering and Pt-oxide–support interaction

Finally, we investigated the essence of the Pt-oxide–support interaction and its relationship to Pt sintering in an oxidizing atmosphere. We tried to consider “on what property of the support does the strength of Pt-oxide–support interaction depend?” As has been pointed out, the Pt–O–M (where M is the cation in the support) bond is key to the Pt-oxide–support interaction. Therefore, it is reasonable to suppose that the electron density of oxygen in the support oxide predominantly influences the strength of the Pt–O–M bond. As a result, the electron density of oxygen in the support would be expected to control the sintering of supported Pt particles. To verify this hypothesis, we conducted a systematic investigation on various Pt-supported

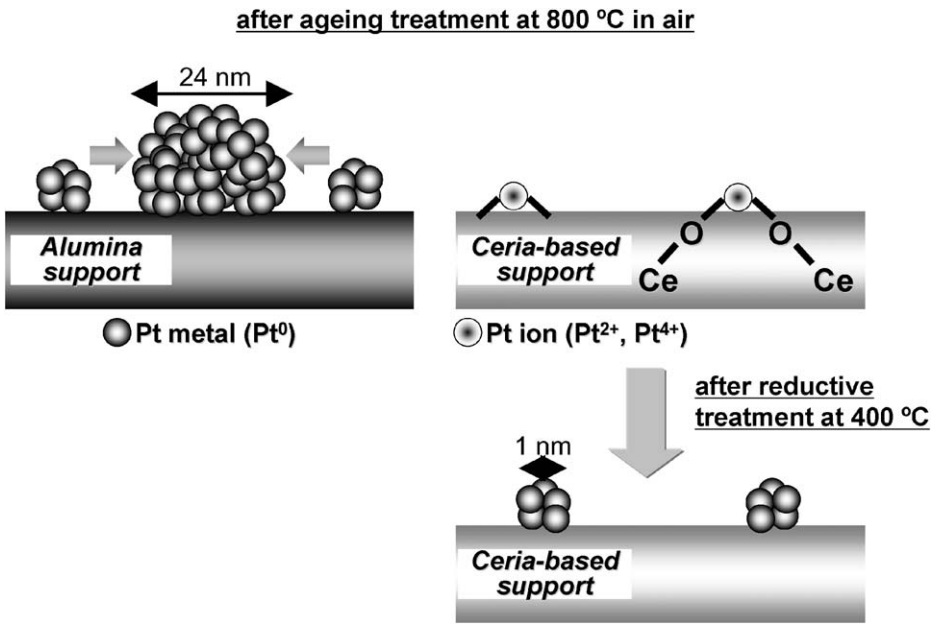

Fig. 6. Model illustration of the Pt sintering inhibition mechanism for a Pt/ceria-based catalyst and a conventional Pt/Al_2O_3 catalyst. Since the Pt–Al_2O_3 interaction is weak, Pt metal particles are formed and sintered during 800 °C aging treatment in air. In contrast, Pt supported on CZY has a strong interaction with CZY support. The generation of Pt–O–Ce bond prevents Pt particles from sintering during the aging treatment. After the reductive treatment, the Pt–O–Ce bond on the CZY breaks, and Pt metal particles are highly dispersed on the support. The average size of Pt metal particles was estimated by a CO pulse adsorption method.

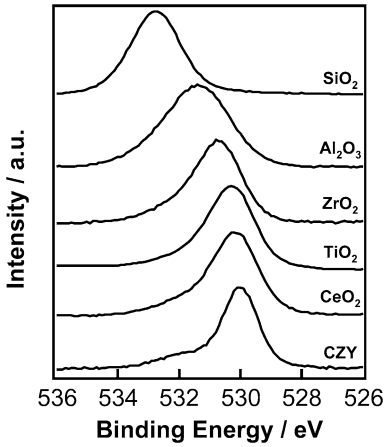

Fig. 7. XPS spectra of the O(1s) core level region in the supports.

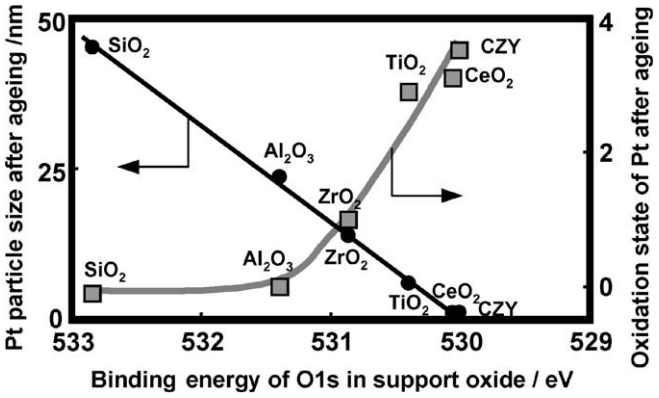

Fig. 8. Pt-oxide–support interaction and its relation to Pt sintering in an oxidizing atmosphere. The binding energy of the O(1s) electron in support oxide was measured by XPS analysis. The oxidation state of Pt after aging was quantitatively evaluated from the white line intensity of the Pt L_3-edge XANES spectra. Pt particle size after aging was estimated by the CO pulse method.

catalysts such as Pt/SiO_2, Pt/TiO_2, and others. Specifically, we quantified the following three properties for various catalysts: the electron density of oxygen in the support, the strength of the Pt-oxide–support interaction, and the sintering inhibition effect on Pt. We also investigated the correlation among these properties. First, in terms of the electron density of oxygen in the support, the binding energy of the O(1s) electron in the support oxide was measured by XPS analysis. XPS spectra of the O(1s) core level region in the supports are given in Fig. 7. Significant changes in the spectra were observed. The binding energy of the O(1s) electron decreased in the following order: SiO_2, Al_2O_3, ZrO_2, TiO_2, CeO_2, and CZY.

Second, concerning quantification of the strength of the Pt-oxide–support interaction, we investigated the white line intensity in the Pt L_3-edge XANES spectra after the aging test in the same way as the Pt/Al_2O_3 and Pt/CZY catalysts. As mentioned above, Pt oxide decomposes to Pt metal under oxidizing conditions at around 600 °C and above. The strong Pt-oxide–support interaction stabilizes the high-oxidation state of Pt through generation of the Pt–O–M bond after aging at 800 °C in an oxidizing atmosphere. Accordingly, it is reasonable to expect the average oxidation state of Pt after aging to correspond to the strength of the Pt-oxide–support interaction. The average oxidation state of Pt can be quantitatively evaluated from the white line intensity in the same way as the Pt/Al_2O_3 and Pt/CZY catalysts.

Third, in terms of the sintering inhibition effect on Pt, we measured the average Pt particle size after the aging at 800 °C in an oxidizing atmosphere. The average size of the Pt metal particles was estimated using the CO pulse method. Fig. 8 shows

the correlations among these three factors on the various supported Pt catalysts. Clearly, these correlations are excellent. The oxidation state of Pt after aging increased with decreasing binding energy of the O(1s) electron. This indicates that the Pt-oxide–support interaction strengthened as the electron density of oxygen of support oxide increased. Subsequently, Pt particle size after the aging decreased as the electron density of oxygen in the support increased. As a result, the sintering inhibition effect on Pt can be controlled by the electron density of oxygen in the support oxide through the Pt-oxide–support interaction. This is the essence of the Pt-oxide–support interaction and its relationship to Pt sintering in an oxidizing atmosphere.

4. Conclusion

Using TEM, XRD, and CO pulse methods, we found that Pt supported on ceria-based oxide (CZY) did not sinter under oxidizing condition at 800 °C, whereas Pt atoms on Al_2O_3 sintered significantly. Pt particles in the Pt/Al_2O_3 grew up to 23.6 nm (by the CO pulse method) during the aging treatment. In contrast, Pt particles in the Pt/CZY after aging continued to be highly dispersed with a diameter of about 1 nm.

Next, we clarified the sintering inhibition mechanism of Pt particles on CZY at the atomic level using XAFS analysis. Pt supported on CZY exhibited a strong interaction with the CZY support; therefore, the CZY support stabilized the high-oxidation state of Pt under oxidizing conditions at high temperatures and then the rigid Pt–O–Ce bond, that is, the Pt-oxide–support interaction generated. The Pt–O–Ce bond acted as an anchor and inhibited Pt migration.

Finally, this report clearly shows the relationship between the inhibitory affect of Pt sintering and Pt-oxide–support interaction. We conducted a systematic investigation on various Pt-supported catalysts and quantified the physical and chemical properties of various catalysts. There was an excellent correlation between the strength of the Pt-oxide–support interaction and the electron density of oxygen in the support oxide. Consequently, it is clear that the sintering inhibition effect on Pt can be controlled by the electron density of oxygen in the support through the Pt-oxide–support interaction.

Using advanced analysis techniques, such as synchrotron radiation-based analysis, the approach to catalytic design for practical use should transit from trial-and-error to planned design and control. We hope that our report can lead the way to the planned catalytic design.

Acknowledgments

The X-ray absorption experiments were performed at the SPring-8 with the approval of the Japan Synchrotron Radiation Research Institute (JASRI). The authors thank Drs. Uruga and Tanida at SPring-8 for the X-ray measurements.

References

[1] S. Matsumoto, Catal. Today 90 (2004) 183.
[2] H.C. Yao, Y.F. Yao, J. Catal. 86 (1984) 254.
[3] M. Ozawa, M. Kimura, A. Isogai, J. Alloys Comp. 193 (1993) 73.
[4] Y. Nagai, T. Yamamoto, T. Tanaka, S. Yoshida, T. Nonaka, T. Okamoto, A. Suda, M. Sugiura, Catal. Today 74 (2002) 225.
[5] P.J.F. Harris, J. Catal. 97 (1986) 527.
[6] R.M.J. Fiedorow, B.S. Chahar, S.E. Wanke, J. Catal. 51 (1978) 193.
[7] C.H. Bartholomew, Appl. Catal. A 212 (2001) 17.
[8] H. Birgersson, L. Eriksson, M. Boutonnet, S.G. Järås, Appl. Catal. B 54 (2004) 193.
[9] E.C. Su, W.G. Rothschild, J. Catal. 99 (1984) 506.
[10] A.F. Diwell, R.R. Rajaram, H.A. Shaw, T.J. Truex, Stud. Surf. Sci. Catal. 71 (2001) 139.
[11] L.L. Murrell, S.J. Tauster, D.R. Anderson, Stud. Surf. Sci. Catal. 71 (2001) 275.
[12] T. Uchijima, Catalytic Science and Technology, Kodansha–VCH, Weinheim, 1990.
[13] A. Holmgren, B. Andersson, D. Duprez, Appl. Catal. B 22 (1999) 215.
[14] T. Tanaka, H. Yamashita, R. Tsutitani, T. Funabiki, S. Yoshida, J. Chem. Soc. Faraday Trans. 84 (1988) 2987.
[15] A.G. McKale, B.W. Veal, A.P. Paulikas, S.K. Chan, G.S. Knapp, J. Am. Chem. Soc. 110 (1988) 3763.
[16] A.N. Mansour, J.W. Cook, D.E. Sayers, J. Phys. Chem. A 88 (1984) 2330.
[17] B.K. Teo, EXAFS: Basic Principles and Data Analysis, Springer-Verlag, Berlin, 1986.
[18] H. Yoshida, S. Nonoyama, Y. Yazawa, T. Hattori, Phys. Scr. T 115 (2005) 813.
[19] S.E. Livingstone, Pergamon Text Inorg. Chem. 25 (1973).
[20] R.B. Greegor, F.W. Lytle, J. Catal. 63 (1980) 476.
[21] R.M.J. Fiedorow, S.E. Wanke, J. Catal. 43 (1976) 34.
[22] P. Forzatti, L. Lietti, Catal. Today 52 (1999) 165.
[23] M. Vaarkamp, Catal. Today 39 (1998) 271.
[24] A.F. Lee, K. Wilson, R.M. Lambert, C.P. Hubbard, R.G. Hurley, R.W. McCabe, H.S. Gandhi, J. Catal. 184 (1999) 491.